Fatigue delamination behavior in composite laminates at different stress ratios and temperatures

Yao, Liaojun; Chuai, Mingyue; Liu, Jurui; Guo, Licheng; Chen, Xiangming; Alderliesten, R. C.; Beyens, M.

DOI
10.1016/j.ijfatigue.2023.107830

Publication date
2023

Document Version
Final published version

Published in
International Journal of Fatigue

International Journal of Fatigue 175 (2023) 107830

Contents lists available at ScienceDirect

International Journal of Fatigue

journal homepage: www.elsevier.com/locate/ijfatigue

Fatigue delamination behavior in composite laminates at different stress ratios and temperatures

Liaojun Yao [a,*], Mingyue Chuai [a], Jurui Liu [a], Licheng Guo [a], Xiangming Chen [b], R.C. Alderliesten [c], M. Beyens [c]

[a] Department of Astronautics Science and Mechanics, Harbin Institute of Technology, Harbin, PR China
[b] AVIC Aircraft Strength Research Institute of China, PR China
[c] Structural Integrity and Composite Group, Faculty of Aerospace Engineering, Delft University of Technology, the Netherlands

ARTICLE INFO

Keywords:
Fatigue delamination
Fibre bridging
R-ratio
Temperature
Composite laminates

ABSTRACT

This study provides an investigation on mode I fatigue delamination growth (FDG) with fibre bridging at different *R*-ratios and temperatures in carbon-fibre reinforced polymer composites. FDG experiments were first conducted at different temperatures of *R*-ratios 0.1 and 0.5 via unidirectional double cantilever beam (DCB) specimens. A fatigue model, employing both the strain energy release rate (*SERR*) range and the maximum *SERR* around crack front as similitude parameter, was proposed to interpret FDG behavior. The use of this model can collapse FDG data with fibre bridging at different *R*-ratios into one master curve, obeying well with the similitude principles. Accordingly, it was found that FDG can accelerate with elevated temperature, but decrease at sub-zero temperature. Furthermore, there are strong correlations between the fatigue model parameters and temperature using this model in FDG interpretations. Taking these correlations into account can extend the model to accurately predict FDG behavior of other temperatures. Fractographic examinations demonstrated that temperature has effects on the FDG damage mechanisms. Both fibre/matrix interfacial debonding and matrix brittle failure were observed in FDG of −40°C. Fibre/matrix interfacial debonding becomes the dominant failure in FDG of RT and 80°C. No obvious difference on the fracture morphology was identified for FDG at different *R*-ratios of a given temperature.

1. Introduction

Fatigue delamination is one of the most important failure modes frequently reported in the application of composite laminates in aeronautic engineering structures, due to the lack of reinforcement in the thickness direction [1–6]. The presence of this damage can have detrimental effects on composite structure integrity (i.e. causing in-plane strength and stiffness reduction), and may potentially lead to catastrophic failure of a composite structure during its operating life [1–3]. Furthermore, the US Federal Aviation Administration (FAA) has introduced the slow-crack growth philosophy in the certification of composite structures since 2009 [7]. As a result, it is critical to have in-depth understanding on FDG behavior, as well as have reliable model to appropriately represent this important failure propagation [8].

Methods based on fracture mechanics have been frequently used in FDG behavior characterization of composite materials, according to the success and experience of using these approaches in fatigue crack growth interpretations of metals [1–4,6,8,9]. Particularly, these models are based on the similitude hypothesis, and mostly expressed in terms of the *SERR* formulation against fatigue crack growth rate *da/dN* [1–2,8].

Paris relation and its variants, based on the similitude hypothesis [9], have been proposed to determine FDG behavior in the previous studies [1–2,8–12]. It has been thoroughly discussed that the application of appropriate parameters obeying the similitude principles plays an important role in appropriately interpreting FDG behavior [12–17]. However, there is no consensus on the *SERR* formulations in representing the similitude. Taking *R*-ratio as an example, the use of the Paris relation Eq.(1), with $\Delta\sqrt{G}$ or G_{max} as similitude parameter, can cause significant and different *R*-ratio dependence on FDG, which indeed violates the basic requirements of similitude principles [12,13,15,16]. From the view of mathematic, a fatigue load cannot be uniquely defined via a single parameter, either $\Delta\sqrt{G}$ or G_{max}. Thus, two-parameter Paris-type relations, employing both $\Delta\sqrt{G}$ and G_{max} in the coupling or uncoupling formulation to represent similitude, have been developed to

* Corresponding author.
E-mail address: L.Yao@hit.edu.cn (L. Yao).

https://doi.org/10.1016/j.ijfatigue.2023.107830
Received 12 April 2023; Received in revised form 15 June 2023; Accepted 6 July 2023
Available online 7 July 2023

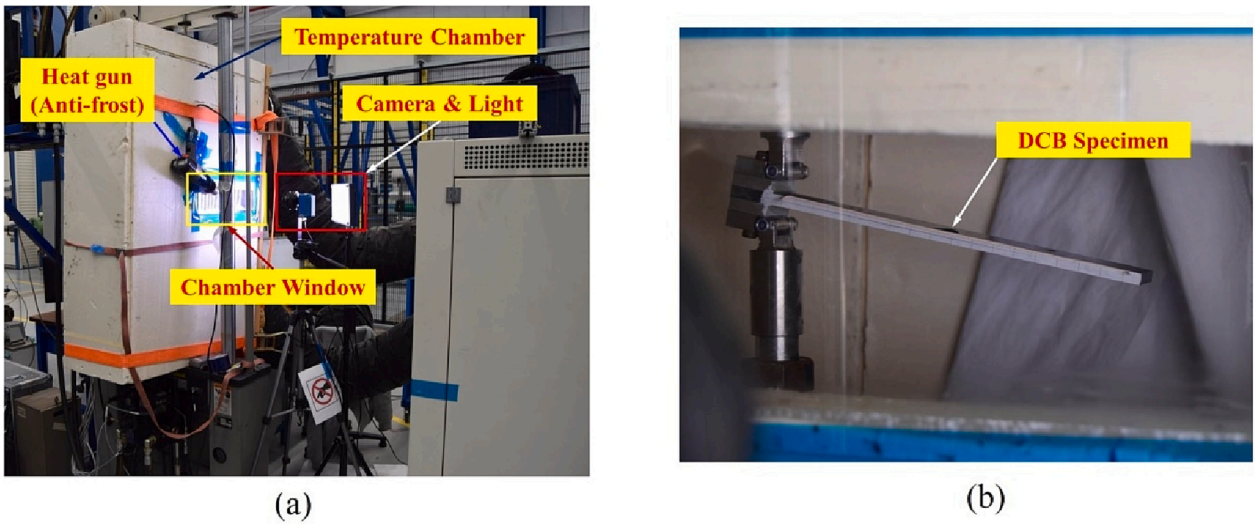

Fig. 1. Experimental setup for FDG test at different temperatures. (a) Overall experimental setup; (b) DCB specimen in the temperature chamber.

Table 1
FDG text matrix at different *R*-ratios and temperatures.

T	Sample	*R*	Fatigue pre-crack propagation a-a_0 [mm]
−40℃	Spe-1	0.1	6.6; 20.7; 35.4; 51.1; 69.8; 86.4; 100.2
	Spe-2	0.5	6.2; 14.6; 22.0; 29.7; 38.2; 47.7; 56.4; 67.3; 78.0; 92.2; 104.0
RT	Spe-3	0.1	5.1; 19.9; 34.9; 53.1; 71.0; 89.4
	Spe-4	0.5	5.1; 14.3; 22.9; 40.7; 53.8; 65.0; 78.9; 92.2
50℃	Spe-5	0.1	6.0; 21.1; 38.7; 57.7; 81.1
	Spe-6	0.5	5.5; 17.5; 29.4; 40.3; 55.1; 67.9; 84.5; 101.9
80℃	Spe-7	0.1	8.5; 24.5; 47.4; 68.0; 90.6
	Spe-8	0.5	7.2; 18.4; 31.4; 43.7; 60.1; 76.3; 92.3; 105.4

determine FDG behavior, in the perspective of fully characterizing a fatigue load [18–21]. The use of these models can collapse FDG data of different stress ratios into a band region, contributing to a single resistance curve in determining FDG behavior, which agrees well with the requirements of similitude principles.

$$\frac{da}{dN} = C\Delta\sqrt{G}^{n} = C\left[\left(\sqrt{G_{\max}} - \sqrt{G_{\min}}\right)^{2}\right]^{n} \; or \; \frac{da}{dN} = CG_{\max}^{n} \tag{1}$$

Fibre bridging is an important and unique shielding mechanism reported several times in FDG of composite laminates in the previous studies [22–27]. The presence of fibre bridging can have significant retardation effects on FDG behavior [22,23]. Hojo et al [28] proposed a $G_{\max}$ constant experimental program and reported that *da/dN* can decrease significantly with fibre bridging development. In another study conducted by the authors [23], it was also reported that the presence of bridging fibres can cause the Paris resistance curves downwards shift with crack propagation (i.e. fibre bridging development). Murri [22] employed both the Paris relation Eq.(1) and the normalized Paris relation (where $G_{\max}$ was normalized by delamination resistance curve) in fibre-bridged FDG interpretations. It was found that the use of this normalized Paris relation can reduce data scatter and have better determination in FDG with fibre bridging. Farmand-Ashtiani et al [25] explored FDG behavior with fibre bridging in composite laminates with different thickness scales. The results indicated that the use of the *SERR* around crack front as similitude parameter can appropriately represent FDG behavior with fibre bridging, which is independent on specimen thickness. Similar conclusion was also made by the authors via energy dissipation and fractographic examination on FDG with fibre bridging [29,30], contributing to a modified Paris relation with similitude parameter $\Delta\sqrt{G_{tip}}$ in interpreting FDG behavior [29]. The use of this relation can make FDG with different amounts of bridging fibres into a narrow band region. As a result, a master resistance curve can be obtained to determine FDG behavior, which agrees well with the similitude principles.

Composite structures can be exposed to a great variety of temperatures in their service life. And it is known that temperature can have important influence on the mechanical properties of both matrix and fibre/matrix interface. These properties indeed directly relate to delamination resistance of composites. As a result, it is crucial to explore FDG behavior at different temperatures and attempt to have reliable model to represent temperature effects on FDG. Researchers [31–36] indeed have conducted fatigue experiments and fractographic examinations to investigate temperature effects on FDG behavior and to reveal the relevant damage mechanisms. Charalambous et al [31] explored mixed-mode I/II FDG behavior of composite IM7/8552 from freezing −50℃ to elevated 80℃ at a given *R*-ratio 0.1. It was found that FDG can increase with elevated temperature but decrease at sub-zero temperature, due to fibre/matrix interfacial debonding is the prominent failure in FDG. Coronado et al [32] provided an experimental study on FDG behavior of two aircraft quality composites (AS4/3501–6 and AS4/8552) at low temperatures from −60℃ to 20℃. The results demonstrated that sub-zero temperature has detrimental effects on FDG behavior. Particularly, FDG rate can accelerate at unfavorable freezing temperatures. The fractographic results indicated that more brittle behavior observed in these composites should be the main reason for this *da/dN* increase at freezing temperatures. Furthermore, in some studies [33–34], it was reported that temperature even can have influence on the generation of fibre bridging in FDG, making the situation even more complex. However, to the best of the authors' knowledge, there is few study conducted to explore FDG behavior with fibre bridging at different temperatures. And there is no reliable model to well represent FDG behavior with fibre bridging at different *R*-ratios and temperatures.

According to above discussions, *R*-ratio, fibre bridging and temperature can have important effects on FDG behavior of composite laminates. The first aim of the present study is therefore to propose a fatigue model to appropriately represent mode I FDG behavior with fibre bridging at different *R*-ratios from sub-zero to elevated temperatures in unidirectional composite laminates. The second objective is to explore the damage mechanisms related to temperature dependence of FDG behavior in composites.

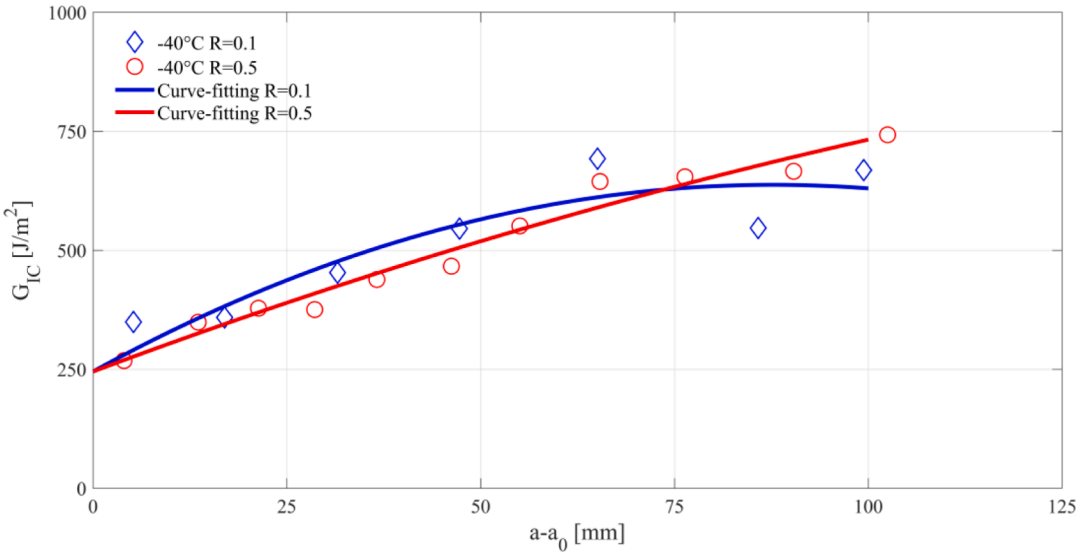

(a)

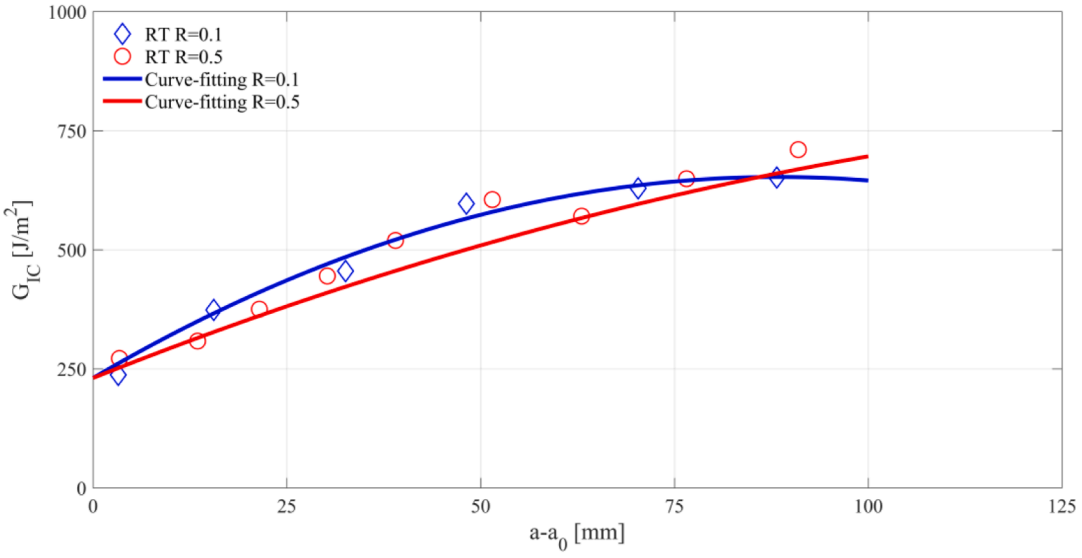

(b)

Fig. 2. Fatigue R-curves of different R-ratios and temperatures. (a) −40 ℃; (b) RT; (c) 80℃.

2. Material, fatigue experiments and data reduction

2.1. Material and specimens

The material used here was carbon fibre/epoxy prepreg M30SC/DT120 (high strength and modulus carbon fibre/toughened thermosetting epoxy). Composite laminates were laid in the designed stacking sequence, i.e. $[0_{16}//0_{16}]$ (// indicates the delamination plane). A Teflon insert with 12.7 μm thickness was placed in the middle plane to introduce an initial delamination, typically around $a_0 = 60$ mm. Laminates were cured in the autoclave at a pressure of 6 bars and curing temperature of 120℃ for 90 min. After curing, the laminates were C-scanned for imperfections. Samples were taken from these areas where no imperfections were identified.

DCB specimens, $L = 200$ mm length by $B = 25$ mm width with thickness of $h = 5$ mm, were cut from the laminates panel with a diamond-coated cutting machine. One side of each DCB specimen was coated with a thin layer of typewriter correction to enhance the visibility of delamination front during fatigue tests. A strip of grid paper was pasted on the coated side of the sample to aid in measuring crack propagation length a-a_0.

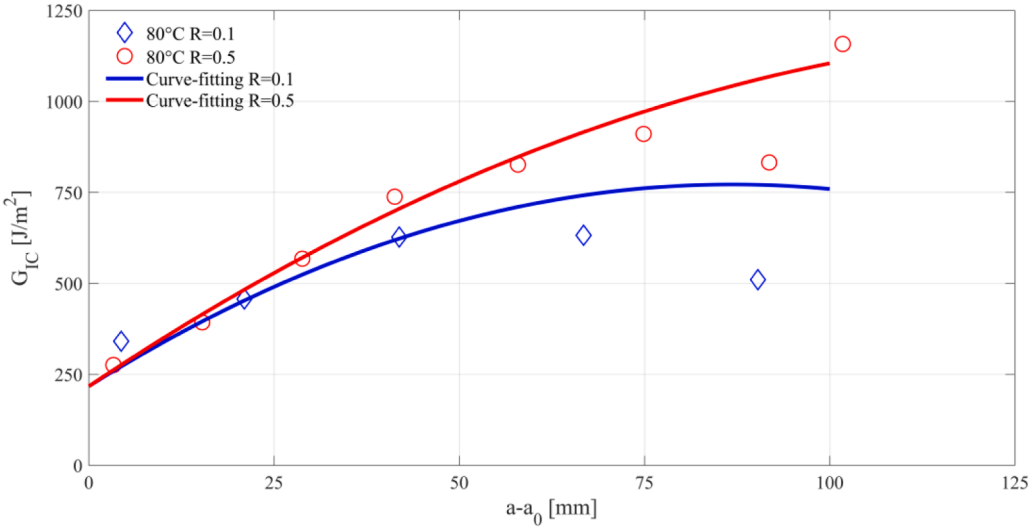

(c)

Fig. 2. (*continued*).

2.2. Fatigue delamination experiments and data reduction

All fatigue experiments were conducted on a 15kN MTS servo-hydraulic test machine under displacement control at a frequency of 5 Hz with stress ratios of $R = 0.1$ and 0.5. The load, displacement and number of cycles were automatically stored in an Excel file, enabling data reduction after the test. A temperature chamber, built in the laboratory with temperature capacity range from −40℃ to 80℃, was used to generate the required temperatures (i.e. −40℃, RT, 50℃ and 80℃) during the entire fatigue tests. Particularly, this chamber contains a window, in front of which a computer controlled digital camera system with high resolution was placed to monitor delamination propagation via automatically recording an image of the tested specimen at certain fatigue intervals. These recorded images could be subsequently analyzed to determine the fatigue delamination propagation length a-a_0 after the experiments. Inside of the chamber, a thermocouple was installed just above the DCB specimen to measure the temperature to ensure there is a stable temperature throughout the entire fatigue test. To keep the monitor window from freezing during fatigue delamination tests at sub-zero temperature, a heat gun was added to act as anti-frost. Detailed information of the experimental setup as well as the DCB specimen in the temperature chamber is demonstrated in Fig. 1.

To determine fatigue delamination behavior with different amounts of fibre bridging, DCB specimens were repeatedly tested for several times with increased displacements keeping the R-ratio constant. This specific test procedure has been introduced and used in the previous studies [23,29,30]. Typically, FDG rate da/dN can gradually decrease with decreasing $SERR$ in a displacement controlled fatigue test. Each test was therefore manually terminated in case of crack retardation. Subsequently, a monotonic loading–unloading cycle was carefully performed on the tested specimen (with certain amount of bridging fibres generated in FDG) until the load–displacement curve becomes slightly nonlinear, to evaluate the interlaminar resistance G_{IC} at the given fatigue crack length and to form the fatigue R-curve $G_{IC}(a\text{-}a_0)$. The maximum and minimum displacements applied in the subsequent fatigue test sequence could be also evaluated via this monotonic loading–unloading cycle. This test sequence was repeated multiple times until the maximum displacement capacity of the test machine was reached. With this specific test procedure, multiple delamination resistance curves could be obtained, with each one representing delamination resistance equivalent to a specific fatigue pre-crack propagation, i.e. delamination length at which that particular fatigue test was initiated.

Table 1 provides a summary of FDG experiments with different fatigue pre-crack propagation (i.e. different amounts of bridging fibres) at different temperatures with different R-ratios. A total number of 58 fatigue delamination experiments were conducted in the present study. Particularly, the fatigue experiments conducted at −40℃, RT and 80℃ were used to verify the validity of the proposed fatigue model in appropriately determining fibre-bridged FDG behavior at different R-ratios and temperatures, and to explore temperature dependence of FDG behavior. The results of 50℃ were used to verify the accuracy of using the proposed fatigue model in predicting FDG behavior of different temperatures.

The Modified Compliance Calibration (MCC) method Eq.(2), recommended in the ASTM D5528 standard [37], was employed to calculate the $SERR$ G with the load, displacement and crack length information recorded in fatigue delamination tests. The 7-point Incremental Polynomial Method, recommended in the ASTM E647 standard [38], was used to fatigue crack growth rate da/dN calculation.

$$G = \frac{3P^2C^{(2/3)}}{2A_1Bh} \tag{2}$$

where P is the load; C is the compliance of the DCB specimen; A_1 is the slope of the curve in the graph where a/h is plotted against $C^{1/3}$.

2.3. Fractographic analysis

Fractographic analysis was conducted using a SEM system JSM-7500F to provide detailed damage mechanism information to interpret temperature effects on FDG behavior. The SEM samples, with 10 mm in length and 25 mm in width, were prepared with gold sputter-coating in vacuum for 10 min to avoid static charging in SEM due to the non-conductive nature of the material used in present study.

3. FDG model development

It has been reported the use of the modified Paris relation Eq.(3) can appropriately interpret fatigue delamination behavior with different

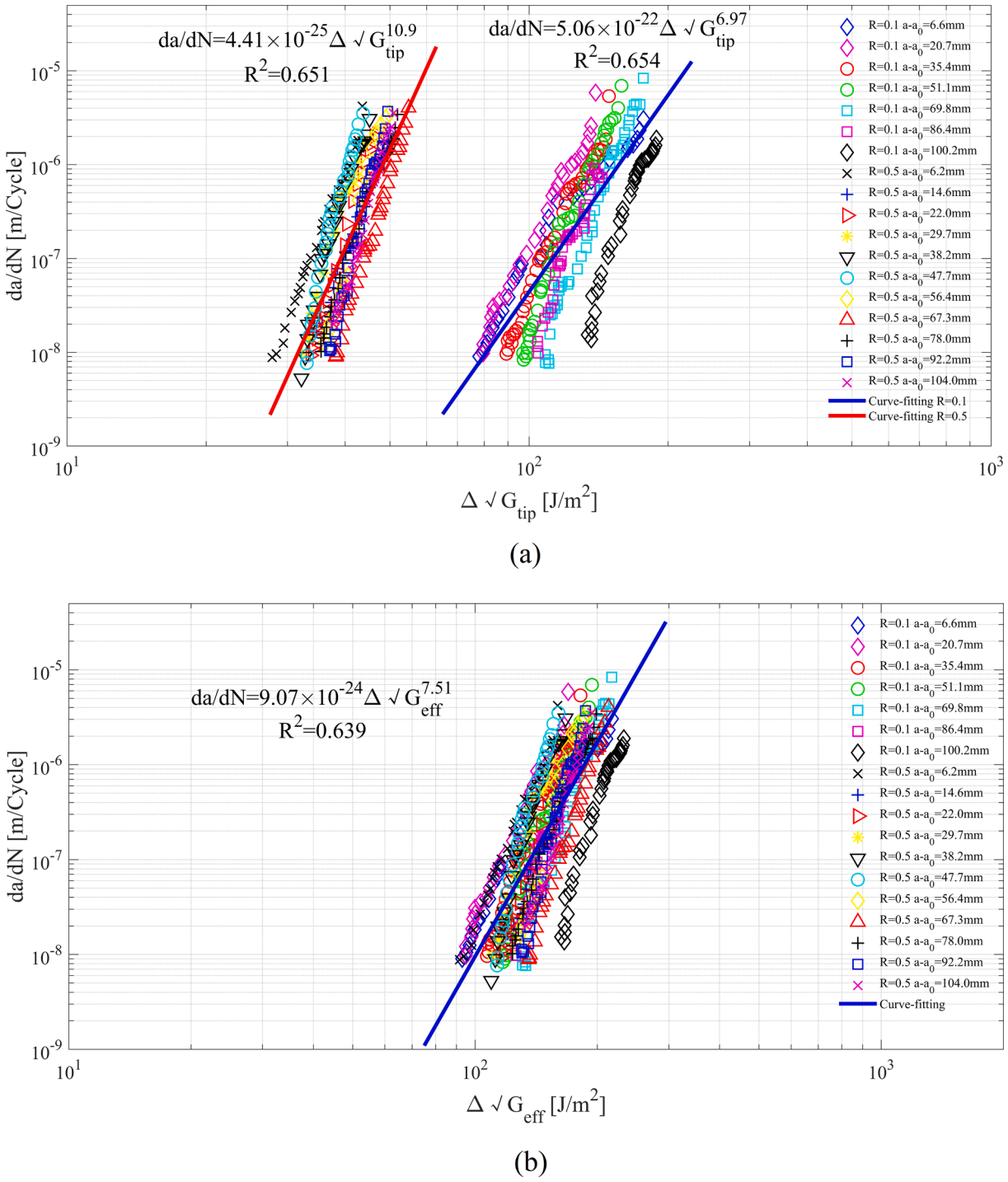

Fig. 3. FDG behavior with fibre bridging at different *R*-ratios of −40 ℃. (a) FDG data interpreted via Eq.(3); (b) FDG data interpreted via Eq.(4).

amounts of bridging fibres in composite laminates at a given *R*-ratios [23,29,30]. A master resistance curve can be calibrated to determine FDG behavior, which is in line with the similitude principles. However, there is still obvious *R*-ratio dependence in FDG interpretations of different *R*-ratios [39]. This means that it is necessary to make further improvements based on Eq.(3) to well represent FDG behavior with the requirements of similitude principles.

$$\frac{da}{dN} = C\Delta\sqrt{G_{tip}}^{n} = C\left[\frac{G_{IC0}}{G_{IC}(a-a_0)}\Delta\sqrt{G}\right]^{n} \tag{3}$$

where $\Delta\sqrt{G_{tip}}$ is the *SERR* range around delamination front; $G_{IC}(a\text{-}a_0)$ represents fatigue resistance increase because of fibre bridging; and G_{IC0} is the fatigue resistance excluding fibre bridging contribution.

According to the concept of fully characterizing a fatigue cycle, as well as the similitude parameter proposed in a recent study accounting for *R*-ratio effects [21], a new fatigue delamination model, employing both $\Delta\sqrt{G_{tip}}$ and G_{max_tip} to represent the similitude, can be developed to characterize FDG behavior with different amounts of bridging fibres at different *R*-ratios as

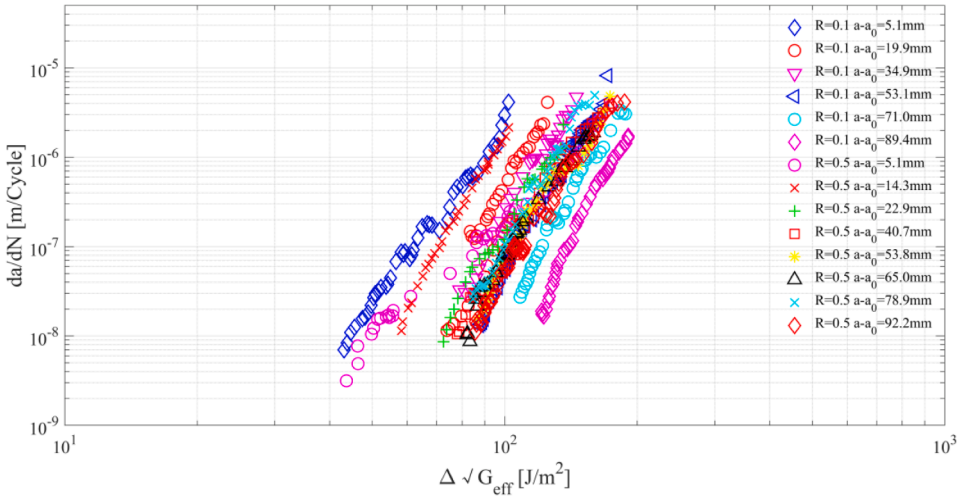

(a)

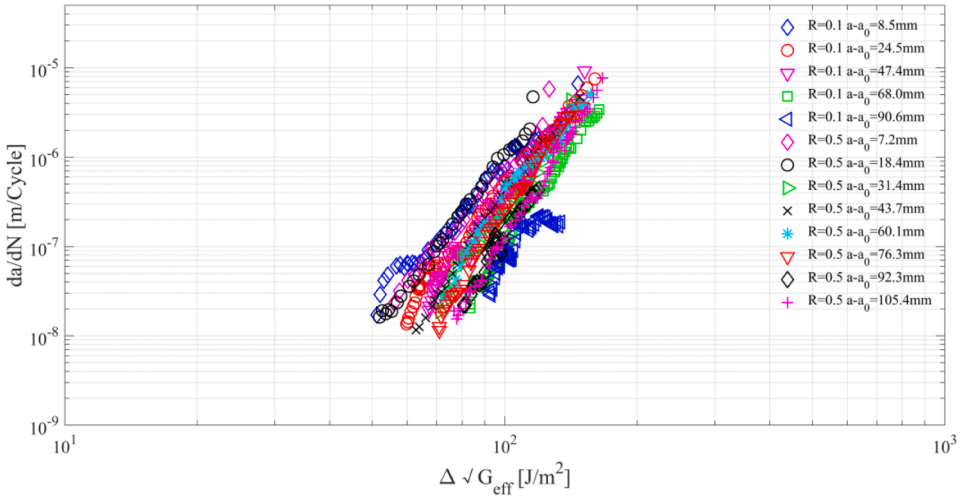

(b)

Fig. 4. FDG behavior at RT and 80℃ with different *R*-ratios. (a) FDG behavior at RT; (b) FDG behavior at 80℃.

$$\frac{da}{dN} = C\Delta\sqrt{G_{eff}}^{n} = C\left[\Delta\sqrt{G_{tip}}\left[1-\left(\frac{G_{\max\_tip}}{G_{IC0}}\right)^{\gamma}\right]G_{\max\_tip}^{\left(\frac{G_{\max\_tip}}{G_{IC0}}\right)^{\gamma}}\right]^{n} \tag{4}$$

where $G_{\max\_tip}$ represents the maximum *SERR* around delamination front, which can be easily determined via Eq.(5); and γ can be best interpreted as the weight-parameter.

$$G_{\max\_tip} = \frac{\Delta\sqrt{G_{tip}}}{(1-R)^{2}} \tag{5}$$

4. Results and discussions

Fatigue data of −40℃, RT and 80℃ were first interpreted via Eq.(4) to verify its validity in determining FDG behavior with fibre bridging at different *R*-ratios, as well as to explore temperature effects on FDG. Accordingly, a detailed discussion on temperature dependence of the fatigue model parameters was conducted to extend the FDG model accounting for temperature effects. Finally, this fatigue model was used to predict FDG behavior with fibre bridging at different *R*-ratios of another temperature 50℃, as the first evidence demonstrating its effectiveness and accuracy.

4.1. Fatigue R-curves of different R-ratios and temperatures

It is necessary to have the fatigue R-curve $G_{IC}(a\text{-}a_0)$ as a prerequisite of using the proposed model Eq.(4) to interpret FDG behavior. With the specific test procedure introduced in Section 2.2, delamination resistance at several fatigue crack lengths can be determined via the MCC method Eq.(2) with the information recorded at the nonlinear point in the monotonic loading–unloading cycle.

Fig. 2 provides a summary of these results in FDG of different *R*-ratios and temperatures. It is clear that delamination resistance can increase significantly with crack propagation, and finally become plateau if the crack propagation is long enough. Fibre bridging is the main reason for

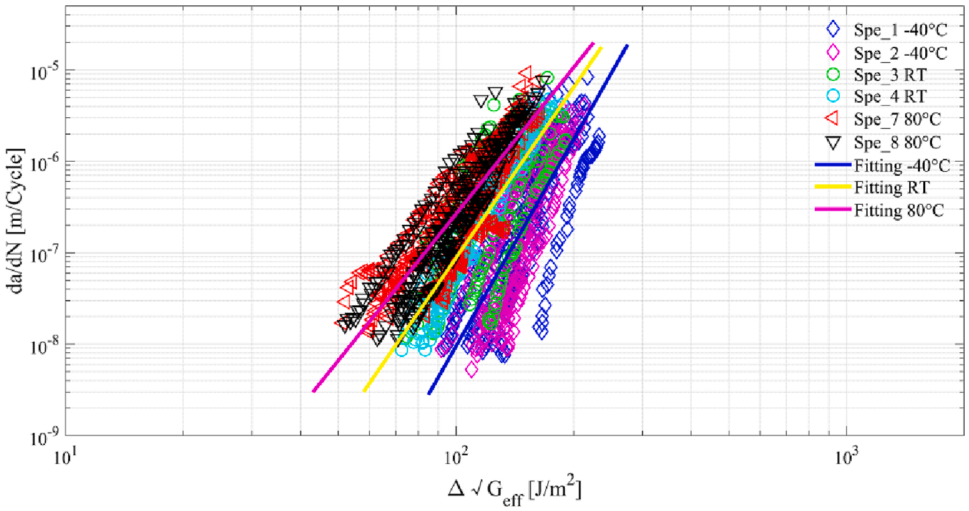

Fig. 5. Temperature effects on FDG behavior.

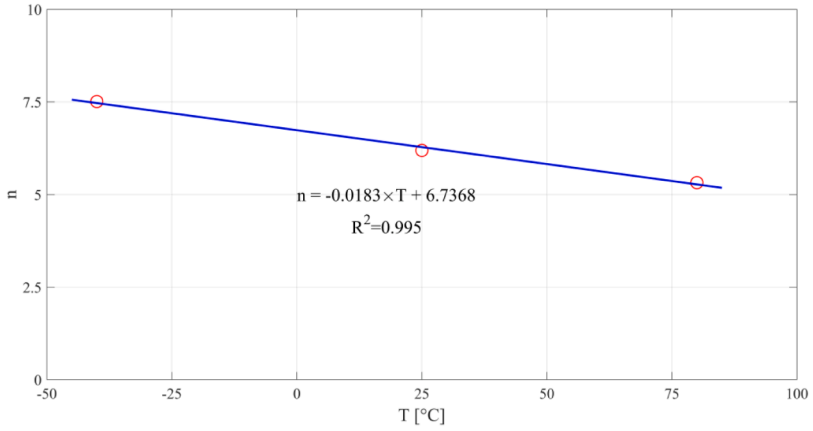

(a)

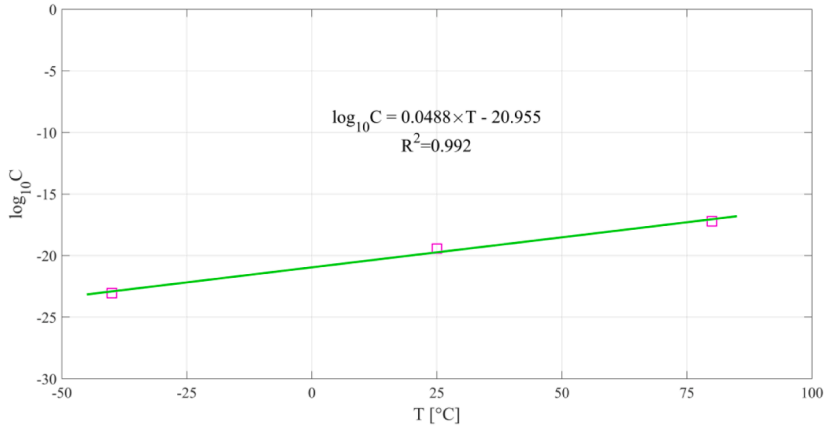

(b)

Fig. 6. Temperature dependence of the fatigue model parameters. (a) n; (b) $log_{10}C$; (c)G_{IC0}; (d) γ.

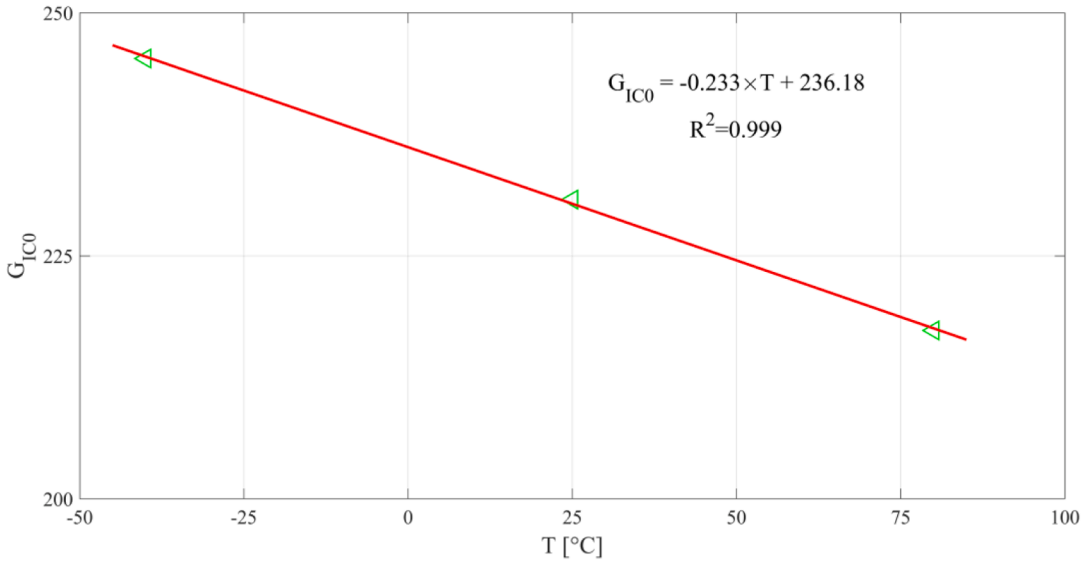

(c)

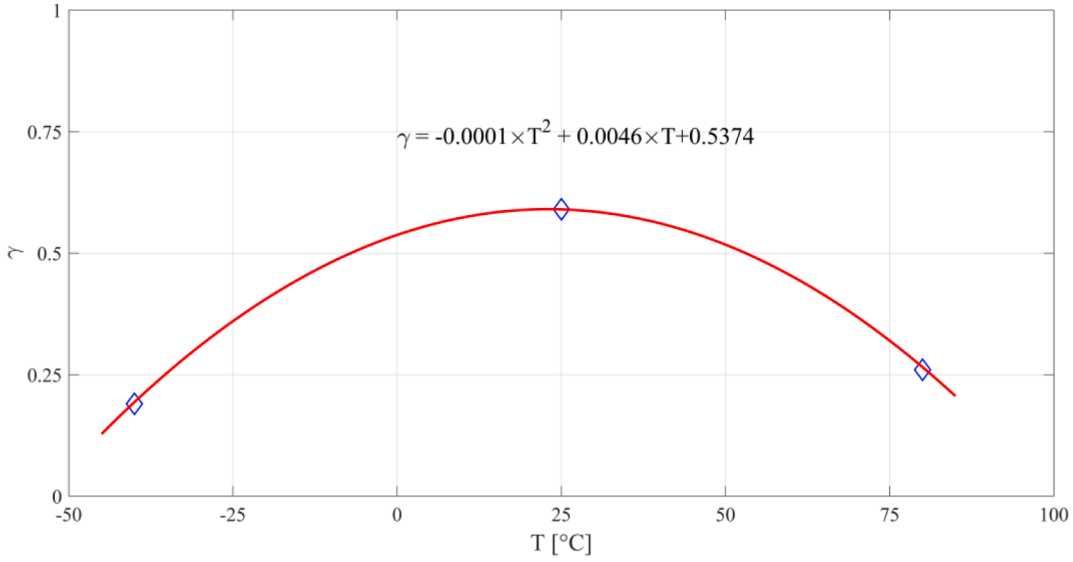

(d)

Fig. 6. (*continued*).

this resistance increase, which has been observed in FDG at all temperatures. With crack growth, more bridging fibres can be present at the behind of crack front, contributing to more energy dissipation of unit crack surface generation. And there is saturation in fibre bridging development, in which the new bridging generation around delamination front can balance with the bridging final failure at the end of bridging zone. Particularly, this resistance increase looks similar for FDG of different *R*-ratios at −40℃ and RT. For 80℃, more bridging fibres can be present in the entire FDG of $R = 0.5$ as compared to $R = 0.1$. And a second-order polynomial function can be fitted to well describe this resistance increase, i.e. $G_{IC}(a\text{-}a_0)$. These fitted results could be subsequently used in Eqs.(3) and (4) for FDG data interpretations.

4.2. FDG behavior with fibre bridging at different R-ratios and temperatures

Taking −40℃ as the first example, both Eqs.(3) and (4) were employed to interpret FDG behavior with fibre bridging at different *R*-ratios. Particularly, Fig. 3(a) provides FDG results interpreted via Eq.(3). The same data sets analyzed via Eq.(4) is given in Fig. 3(b). It is clear that the use of $\Delta\sqrt{G_{tip}}$ as similitude parameter can appropriately represent the similarity in fibre-bridged FDG. In other words, FDG behavior with different amounts of bridging fibres for a given *R*-ratio can converge into a narrow band region, contributing to a master resistance curve in determining FDG behavior, which agrees well with the requirements of the similitude hypothesis. However, there is still

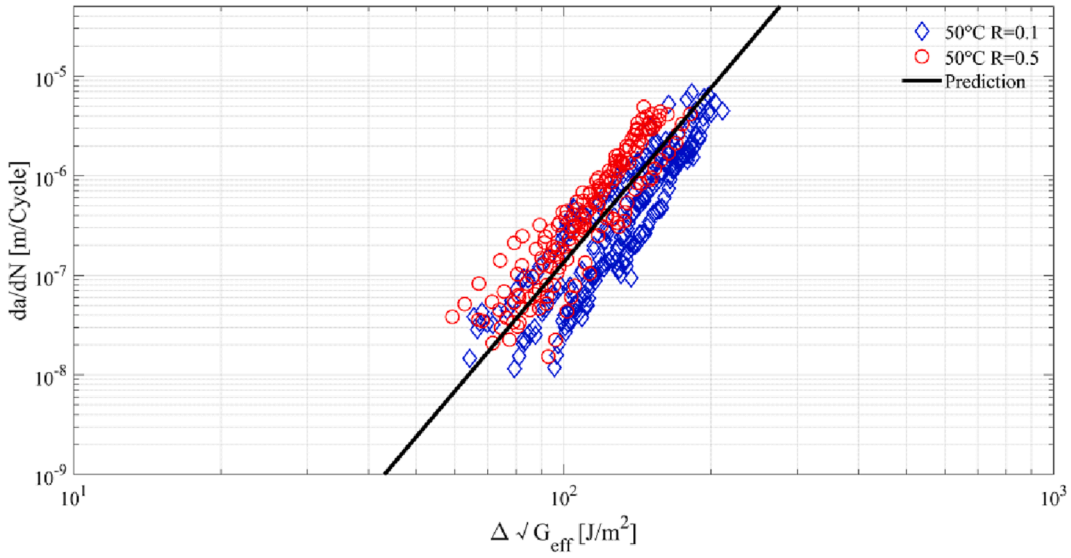

Fig. 7. FDG predictions of 50°C.

obvious R-ratio dependence in fatigue delamination interpretations using Eq.(3). And FDG rate of $R = 0.5$ is much higher than that of $R = 0.1$ for the same $\Delta\sqrt{G_{tip}}$. On the contrary, all fatigue data with different amounts of bridging fibres at various R-ratios can collapse into a band region once using the proposed model Eq.(4) in data reduction as illustrated in Fig. 3(b). As a result, a master resistance curve can be calibrated to appropriately represent FDG behavior regardless of R-ratios, obeying well with the similitude principles.

The results illustrated in Fig. 3 can provide the first evidence on the validity of using Eq.(4) in appropriately determining FDG behavior with fibre bridging at different R-ratios. These results also highlight the importance of employing an appropriate similitude parameter in FDG data interpretations.

To have more evidence on the validity of using this proposed model Eq.(4), fatigue delamination data of RT and 80℃ at different R-ratios were respectively analyzed as shown in Fig. 4. Despite some scatter is observed in data reduction of RT, it is clear that the use of this proposed model can well account for both fibre bridging and R-ratio effects on FDG. In other words, fatigue delamination with different amounts of bridging fibres at various R-ratios tend to collapse into a band region, leading to a master resistance curve in determining FDG behavior. It is therefore possible to make a comparison on temperature effects on fibre-bridged FDG behavior via fatigue data interpretations with Eq.(4).

Data scatter is an important and inevitable issue frequently reported in fatigue delamination study. As discussed in literature [40–41], the sources of scatter can be divided into intrinsic and extrinsic. The extrinsic scatter includes test set-up, operator experience, specimen preparation, cutting quality, variation in laminate thickness and so on. The intrinsic scatter, related to inhomogeneous material morphology and process variability, can also have obvious effects on fatigue delamination scatter. Particularly, fibre bridging, observed in FDG of the present study, can constitute a source of intrinsic scatter [40]. To the authors' opinion, all above mentioned factors can have contribution to data scatter observed in fatigue delamination experiments.

Fig. 5 summarizes all fatigue data with fibre bridging of different R-ratios and temperatures in terms of da/dN against $\Delta\sqrt{G_{eff}}$. The corresponding resistance curves were also fitted to represent FDG behavior. It is clear that FDG behavior can accelerated with elevated temperature 80℃, but decrease at sub-zero temperature −40℃. Another important feature is that the slope of these resistance curves will decrease with increased temperatures. As discussed in [31], this slope decrease is related to matrix ductility increase. At freezing temperature −40℃, matrix becomes even brittle, leading to a steeper FDG resistance curve.

4.3. FDG behavior prediction

All above discussions clearly demonstrate that the proposed fatigue model Eq.(4) can well interpret mode I FDG behavior with fibre bridging at different R-ratios and temperatures of unidirectional composite laminates. People may then ask a question that how about of using this calibrated Eq.(4) in determining FDG behavior with fibre bridging of other temperatures.

To this aim, a further discussion on temperature dependence of the fatigue model parameters, i.e. n, $log_{10}C$, G_{IC0} and γ, were conducted via the fitted results illustrated in Fig. 5. Interestingly, there are strong linear correlations between these parameters of $log_{10}C$, n, G_{IC0} and temperature T, as shown in Fig. 6 (a) to (c). And a non-monotonic relation is observed between γ and temperature T, as shown in Fig. 6 (d). Taking these correlations into account can extend Eq.(4) as

$$\frac{da}{dN} = C(T)\left[\Delta\sqrt{G_{tip}}\left[1-\left[\frac{G_{\max\_tip}}{G_{IC0}(T)}\right]^{\gamma(T)}\right]G_{\max\_tip}\left[\frac{G_{\max\_tip}}{G_{IC0}(T)}\right]^{\gamma(T)}\right]^{n(T)} \quad (6)$$

For the calibrated Eq.(6), one may ask a question like this: how about its validity in determining FDG behavior. Another group of FDG experiments conducted at 50℃ with different R-ratios 0.1 and 0.5 were thus used here to verify its effectiveness and accuracy. Fig. 7 summarizes all fatigue delamination data interpreted via Eq.(4) and the corresponding predicted resistance curve via the calibrated Eq.(6). First, it is clear that the use of the proposed model Eq.(4) can well interpret FDG behavior with fibre bridging at different R-ratios. All fatigue data can collapse into a band region, agreeing well with the similitude principles. Secondly, the use of the calibrated Eq.(6) can accurately determine FDG behavior with fibre bridging of different R-ratios at 50℃. Particularly, the predicted resistance curve can pass through the central part of these experimental data in the entire da/dN magnitudes.

Accordingly, it can be concluded that the proposed fatigue model can well interpret and predict mode I fatigue delamination behavior with fibre bridging at different R-ratios and temperatures of unidirectional composite laminates. Furthermore, it is worth highlighting that the use of this model in FDG interpretations has great potential to significantly reduce experimental workload and time-consuming, which is really useful and important for composite structural design and life evaluation.

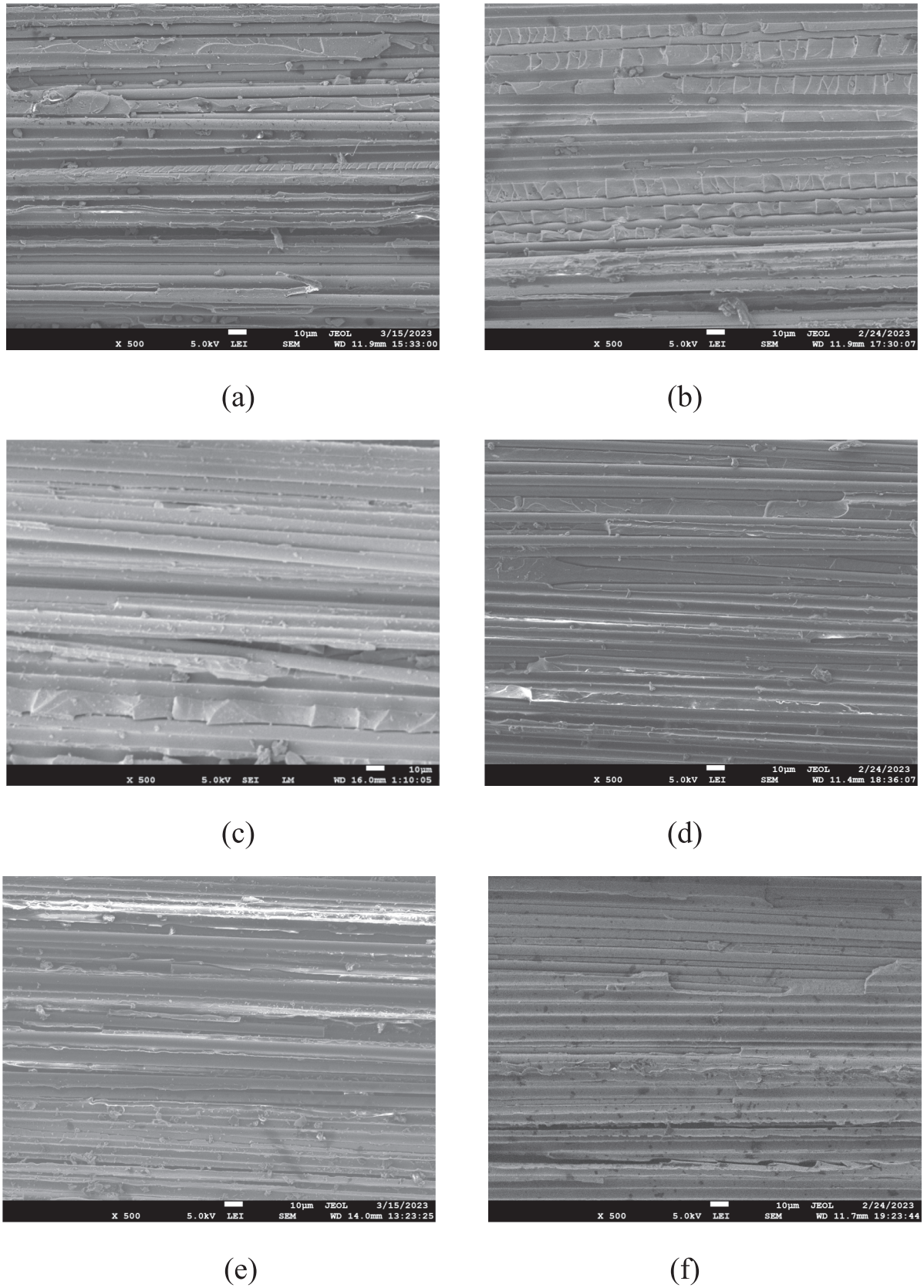

Fig. 8. Fatigue fracture morphologies at −40 ℃, RT and 80 ℃ of *R*-ratios 0.1 and 0.5. (a) −40 ℃ $R = 0.1$; (b) −40 ℃ $R = 0.5$; (c) RT $R = 0.1$; (d) RT $R = 0.5$; (e) 80 ℃ $R = 0.1$; (f) 80 ℃ $R = 0.5$.

4.4. Fractographic analysis on fatigue delamination surfaces

As discussed in the previous study [29,30], fibre/matrix interfacial debonding is the dominant failure mechanism in FDG of composite M30SC/DT120 at RT. This failure can cause obvious fibre prints distributed on fatigue fracture surface. Fig. 8 gives SEM examinations on fatigue delamination surfaces at −40℃, RT and 80℃. It can be found that both fibre/matrix debonding (identified by obvious fibre prints) and matrix brittle fracture (indicated by river markings and hackles) can be clearly observed on delamination surfaces of −40℃. However, fibre/matrix interfacial debonding becomes more dominate at RT and 80℃, and no obvious matrix brittle damage is found on the fracture surfaces.

The fracture morphology for FDG at different *R*-ratios of a given temperature generally remains the same. For −40℃, both fibre prints and hackles are typical microscopic features observed on fatigue delamination surfaces, whereas for RT and 80℃ fibre prints become the dominant microscopic feature distributed on fracture surfaces of different *R*-ratios.

Due to the difference in the coefficients of thermal expansion between reinforced carbon-fibre and the matrix, freezing temperature can enhance interfacial bond performance via interlocking mechanism [31,42]. This can cause more energy dissipation during FDG at −40℃, contributing to obvious reduction in *da/dN*. Elevated temperature can not only have detrimental effects interfacial adhesion behavior, but may also promote more matrix plastic deformation under cyclic loading, and therefore increase the possibility of micro-crack generation and macro-delamination growth [31,34]. As a result, FDG behavior of 80℃ is much faster than that of RT and −40℃.

5. Concluding remarks

A fatigue model has been developed to interpret mode I FDG behavior with fibre bridging at different *R*-ratios and temperatures of unidirectional composite laminates. The use of this model can collapse fatigue delamination data into a band region, contributing to a master resistance curve in representing FDG behavior with fibre bridging at different *R*-ratios and temperatures. These results clearly demonstrate that FDG behavior can accelerate with elevated temperature, but decrease at sub-zero temperature.

It was found that there are strong correlations between the fatigue model parameters and temperature using this proposed model in mode I FDG interpretations. Taking these correlations into account can extend the fatigue model to accurately determine FDG behavior of other temperatures. As a result, the application of this model in FDG interpretations has great potential to significantly reduce experimental workload and time-consuming, which is really useful for composite structural design and life evaluation.

Fractographic examinations on fatigue fracture surfaces of different temperatures indicate that temperature has important influence on fatigue delamination damage mechanisms. Particularly, fibre/matrix interfacial debonding and matrix brittle fracture are the dominate failure modes in FDG at sub-zero temperature, as significant fibre prints and river markings are observed on delamination surfaces. For RT and elevated 80℃, fibre/matrix interfacial debonding is the dominant failure mechanism.

Referring to the round-robin test programs organized by the European Structural Integrity Society Technical Committee 4 (ESIS TC-4) [10,11], this study can not only provide material database, but also give insights for developing mode I fatigue delamination test standard of composite materials.

CRediT authorship contribution statement

Liaojun Yao: Conceptualization, Methodology, Software, Validation, Formal analysis, Investigation, Resources, Data curation, Writing – original draft, Writing – review & editing, Visualization, Supervision, Project administration, Funding acquisition. **Mingyue Chuai:** Software, Validation, Formal analysis, Visualization. **Jurui Liu:** Methodology, Software, Validation. **Licheng Guo:** Formal analysis, Data curation. **Xiangming Chen:** Formal analysis, Data curation. **R.C. Alderliesten:** Methodology, Data curation. **M. Beyens:** Methodology, Software, Data curation.

Declaration of Competing Interest

The authors declare that they have no known competing financial interests or personal relationships that could have appeared to influence the work reported in this paper.

Data availability

Data will be made available on request.

Acknowledgement

The authors gratefully acknowledge financial support from the National Natural Science Foundation of China with Grant No. 11902098, 12272110 and 12272358, the Aeronautical Science Foundation of China with Grant No. 20200009077001, the Natural Science Foundation of Heilongjiang Province with Grant No. LH2020A005.

References

[1] Bak BLV, Sarrado C, Turon A, Costa J. Delamination under fatigue loads in composite laminates: a review on the observed phenomenology and computational methods. Appl Mech Rev 2014;060803.
[2] Khan R, Alderliesten R, Badshah S, Benedictus R. Effect of stress ratio or mean stress on fatigue delamination growth in composites: critical review. Compos Struct 2015;124:214–27.
[3] Mamalis D, Floreani C, Bradaigh CMO. Influence of hygrothermal ageing on the mechanical properties of unidirectional carbon fibre reinforced powder epoxy composites. Compos B Eng 2021;225:109281.
[4] Jensen SM, Bak BLV, Bender JJ, Lindgaard E. Transition-behaviours in fatigue-driven delamination of GFRP laminates following step changes in block amplitude loading. Int J Fatigue 2021;144:106045.
[5] Mueller EM, Starnes S, Strickland N, Kenny P, Williams C. The detection, inspection, and failure analysis of a composite wing skin defect on a tactical aircraft. Compos Struct 2016;145:186–93.
[6] Jones R, Pitt S, Bunner AJ, Hui D. Application of the Hartman-Schijve equation to represent mode I and mode II fatigue delamination growth in composites. Compos Struct 2012;94:1343–51.
[7] Federal Aviation Authority. Airworthiness advisor circular No: 20-107B. Composite Aircraft Structure 2009.
[8] Pascoe JA, Alderliesten RC, Benedictus R. Methods for the prediction of fatigue delamination growth in composites and adhesive bonds – a critical review. Eng Fract Mech 2013;112–113:72–96.
[9] Jones R, Molent L, Pitt S. Similitude and the Paris crack growth law. Int J Fatigue 2008;30:1873–80.
[10] Stelzer S, Brunner AJ, Arguelles A, et al. Mode I delamination fatigue crack growth in unidirectional fiber reinforced composites: Development of a standardized test procedure. Compos Sci Technol 2012;72:1102–7.
[11] Stelzer S, Brunner AJ, Arguelles A, et al. Mode I delamination fatigue crack growth in unidirectional fiber reinforced composites: Results from ESIS TC 4 round-robins. Eng Fract Mech 2014;116:92–107.
[12] Cano AJ, Salazar A, Rodriguez J. Evaluation of different crack driving forces for describing the fatigue crack growth behavior of PET-G. Int J Fatigue 2018;107:27–32.
[13] Rans C, Alderliesten R, Benedictus R. Misinterpreting the results: How similitude can improve our understanding of fatigue delamination growth. Compos Sci Technol 2011;71:230–8.
[14] Alderliesten RC. How proper similitude can improve our understanding of crack closure and plasticity in fatigue. Int J Fatigue 2016;82:263–73.
[15] Jones R, Kinloch AJ, Hu W. Cyclic-fatigue crack growth in composite and adhesively-bonded structures: The FAA slow crack growth approach to certification and the problem of similitude. Int J Fatigue 2016;88:10–8.
[16] Simon I, Banks-Sills L, Fourman V. Mode I delamination propagation and R-ratio effects in woven composite DCB specimens for a multi-directional layup. Int J Fatigue 2017;96:237–51.
[17] Jones R, Kinloch AJ, Michopoulos J, Iliopoulos AP. Crack growth in adhesives: Similitude and the Hartman-Schijve equation. Compos Struct 2021;273:114260.
[18] Hojo M, Tanaka K, Gustafson CG, Hayashi R. Effect of stress ratio on near-threshold propagation of delamination fatigue cracks in unidirectional CFRP. Compos Sci Technol 1987;29:273–92.

[19] Atodaria DR, Putatunda SK, Mallick PK. Delamination growth behavior of a fabric reinforced laminated composite under mode I fatigue. J Eng Mater Technol 1999; 121:381–5.
[20] Khan R, Alderliesten R, Benedictus R. Two-parameter model for delamination growth under mode I fatigue loading (Part A: Experimental study). Compos A Appl Sci Manuf 2014;65:192–200.
[21] Yao L, Cui H, Guo L, Sun Y. A novel total fatigue life model for delamination growth in composite laminates under generic loading. Compos Struct 2021;258: 113402.
[22] Murri GB. Effect of data reduction and fiber-bridging on mode I delamination characterization of unidirectional composites. J Compos Mater 2014;2413–2424.
[23] Yao L, Cui H, Sun Y, et al. Fibre-bridged fatigue delamination in multidirectional composite laminates. Compos A Appl Sci Manuf 2018;115:175–86.
[24] Donough MJ, Gunnion AJ, Orifici AC, Wang CH. Scaling parameter for fatigue delamination growth in composites under varying load ratios. Compos Sci Technol 2015;120:39–48.
[25] Framand-Ashtiani E, Cugnoni J, Botsis J. Effects of large scale bridging in load controlled fatigue delamination of unidirectional carbon-epoxy specimens. Compos Sci Technol 2016;137:52–9.
[26] Zhao L, Gong Y, Zhang J, et al. A novel interpretation of fatigue delamination growth behavior in CFRP multidirectional laminates. Compos Sci Technol 2016; 133:79–88.
[27] Jensen SM, Bak BLV, Bender JJ, Carreras L, Lindgaard E. Transient delamination growth in GFRP laminates with fibre bridging under variable amplitude loading in G-control. Compos B Eng 2021;225:109296.
[28] Hojo M, Ando T, Tanaka M, et al. Mode I and Mode II interlaminar fracture toughness and fatigue delamination of CF/epoxy laminates with self-same epoxy interleaf. Int J Fatigue 2006;28:1154–65.
[29] Yao L, Sun Y, Guo L, et al. A modified Paris relation for fatigue delamination with fibre bridging in composite laminates. Compos Struct 2017;176:556.564.
[30] Yao L, Cui H, Alderliesten RC, Sun Y, Guo L. Thickness effects on fibre-bridged fatigue delamination growth in composites. Compos A Appl Sci Manuf 2018;110: 21–8.
[31] Charalambous G, Allegri G, Hallett SR. Temperature effects on mixed mode I/II delamination under quasi-static and fatigue loading of a carbon/epoxy composite. Compos A Appl Sci Manuf 2015;77:75–86.
[32] Coronado P, Arguelles A, Vina J, Vina I. Influence of low temperatures on the phenomenon of delamination of mode I fracture in carbon-fibre/epoxy composites under fatigue loading. Compos Struct 2014;112:188–93.
[33] Gregory JR, Spearing SM. A fiber bridging model for fatigue delamination in composite materials. Acta Mater 2004;52:5493–502.
[34] Gregory JR, Spearing SM. Constituent and composite quasi-static and fatigue fracture experiments. Compos A Appl Sci Manuf 2005;36:665–74.
[35] Sjogren A, Asp LE. Effects of temperature on delamination growth in a carbon/ epoxy composite under fatigue loading. Int J Fatigue 2002;24:179–84.
[36] Shindo Y, Inamoto A, Narita F, et al. Mode I fatigue delamination growth in GFRP woven laminates at low temperatures. Eng Fract Mech 2006;73:2080–90.
[37] ASTM D5528-01. Standard test method for mode I interlaminar fracture toughness of unidirectional fiber-reinforced polymer matrix composites. American Society for Testing and Materials, 2007.
[38] ASTM E647-00. Standard test method for measurement of fatigue crack growth rates. American Society for Testing and Materials, 2001.
[39] Yao L, Sun Y, Guo L, et al. A validation of a modified Paris relation for fatigue delamination growth in unidirectional composite laminates. Compos B Eng 2018; 132:97–106.
[40] Alderliesten RC, Brunner AJ, Pascoe JA. Cyclic fatigue fracture of composites: What has testing revealed about the physics of processes so far? Eng Fract Mech 2018;203:186–96.
[41] Brunner AJ. Fracture mechanics testing of fiber-reinforced polymer composites: the effects of the “human factor” on repeatability and reproducibility of test data. Eng Fract Mech 2022;264:108340.
[42] Hartwig G, Knaak S. Fibre-epoxy composites at low temperature. Cryogenics 1984; 24:639–47.